Photo of Arenal volcano (Costa Rica) by **Dimitri Sokolenko**

T21A-4558

Mongolian Hangay Uplift Recorded in Vesicular Basalts

D. Sahagian
dork.sahagian@lehigh.edu
Earth and Environmental Sciences
Lehigh University,
STEPS 424, Bethlehem, PA 18015

A. Proussevitch
alex.proussevitch@unh.edu
Earth Systems Research Center
University of New Hampshire
Durham, NH 03824

L. Ancuta
lda210@lehigh.edu
Earth and Environmental Sciences
Lehigh University,
STEPS 424, Bethlehem, PA 18015

B. Idleman
bdi2@lehigh.edu
Earth and Environmental Sciences
Lehigh University,
STEPS 424, Bethlehem, PA 18015

P. Zeitler
peter.zeitler@lehigh.edu
Earth and Environmental Sciences
Lehigh University,
STEPS 424, Bethlehem, PA 18015

Abstract

Epeirogenic histories of highland areas have confounded geophysicists for decades, as there are few records of paleoelevation in eroding highlands. However, preserved basaltic lava flows record paleoelevation in the size distributions of vesicles at the tops and bottoms of flow units. Although the bubbles have identical mass distributions at top and base, they are subject to different total pressures due to differences in overburden. At the top of the flow, only the overlying atmospheric exerts pressure, Patm, whereas at the base, the lava itself exerts pressure as a function of its thickness, H. Consequently, two factors control the size of bubbles at the base of the flow: atmospheric pressure and lava weight. Thus, the atmospheric pressure-dependence of vesicle size can be expressed by the ratio of vesicle size modes at the top and bottom of a flow. The atmosphere's paleopressure can thus be determined, because all other variables can be measured, and based on the known relationship of pressure as a function of elevation, a paleoelevation can then be calculated. Knowing the elevation at which the rock formed, its age, and its present elevation, the amount of uplift or subsidence can be determined, providing a history of tectonic uplift or subsidence of the locality. As with any proxy for paleoelevation, there are numerous limitations and error sources. These include the possibility that the lava was inflated of deflated after solidification of vesicular top and bottom, errors in flow thickness measurement, variations in atmospheric pressure during solidification, the presence or absence of large vesicles in sample cores, and many other minor sources. The total error bounds of the method are estimated to be ±400 m, which is sufficient only for major epeirogenic trends, such as that seen previously on the Colorado Plateau, and now in Mongolia.

As part of a broader collaborative project, we collected samples from several flows from throughout the Hangay Plateau. Results indicate that Hangay experienced uplift of over 1 km in the last 10 Ma at a rate of about 140 m/Ma. A flow sampled from the neighboring Gobi Desert indicates a paleoelevation of only a few hundred m, suggesting that the Hangay Plateau uplifted independently from the regions to the south, which have not experienced the same tectonics as Hangay over the past 20 m.y. The uplift history of Hangay, in addition to the composition of the lavas, geomorphology of the region, drainage pattern history, and other proxies, bears on possible mechanisms for uplift of this part of central Asia, now being explored.

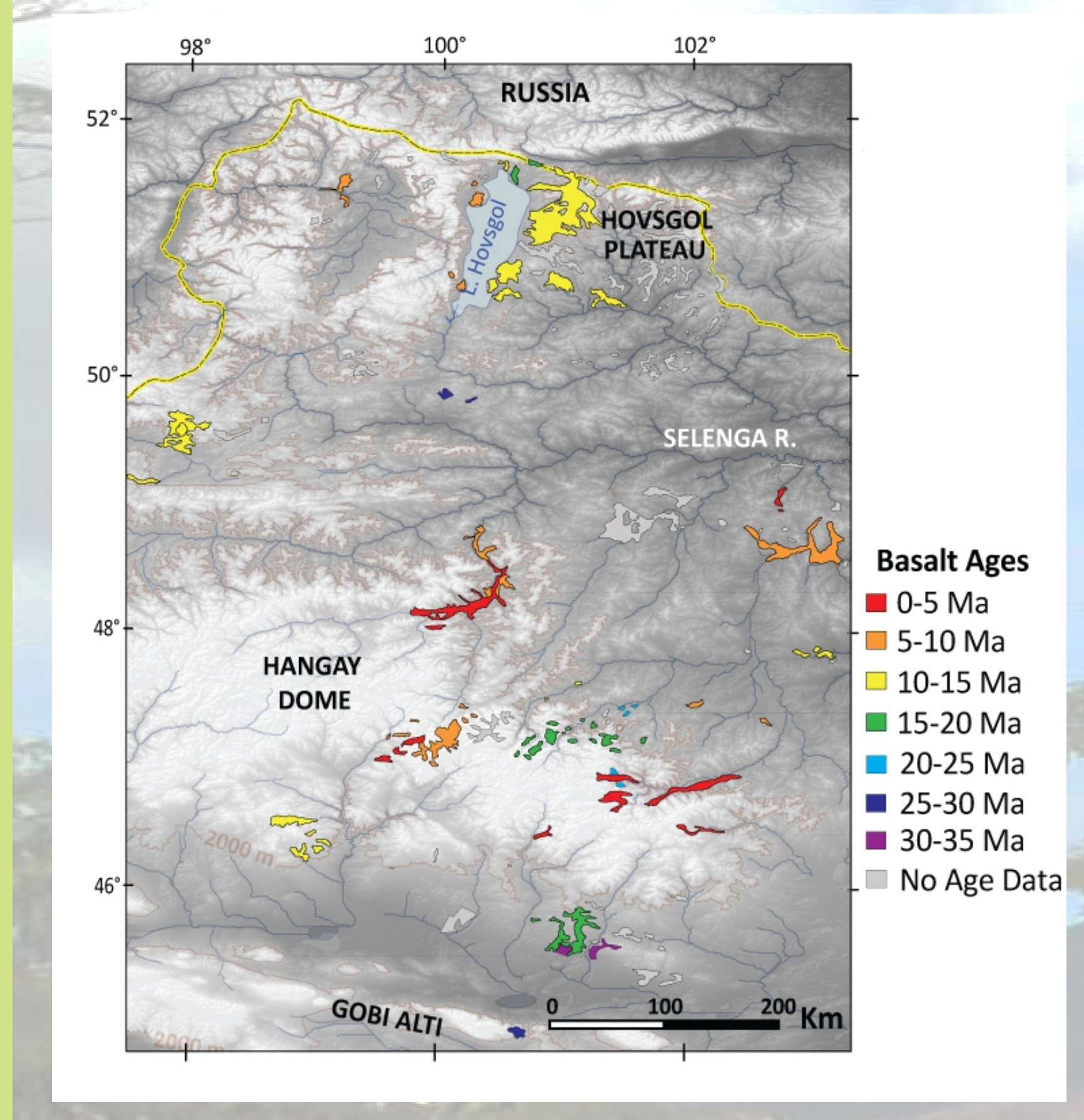

Introduction

Numerous major plateaus have emerged within the various continents, yet the driving mechanisms for uplift remain unclear in many cases. Explanations proposed for their origin have been as diverse as their tectonic settings, and include dynamic topography supported by deep-mantle plumes, asthenospheric upwelling driven by various mechanisms, basaltic underplating, thickened crustal wedges, and various forms of lithospheric "drips" involving foundering or delamination of mantle or crustal lithosphere.

The interior of the Hangay Dome in Mongolia locally reaches elevations over 4000 m and contains high-elevation low-relief topography interpreted as an uplifted and well-preserved paleo-erosional surface of presumed Late Cretaceous age, cut into Precambrian basement rocks, Paleozoic strata and Permian and Jurassic granitoids. Geological and geomorphic evidence suggest uplift, faulting, and volcanism are fairly recent, although when and why these processes initiated or how they relate in space and time are poorly known. Consequently, we are using methods such paleotopography, geomorphology, drainage basin identification, age dating of volcanics, and seismics to shed light on the mechanism(s) of plateau uplift. **In order to determine the timing of uplift of the plateau, we used vesicular basalt flows as a measure of atmospheric pressure at the time of eruption, and thus as a proxy for paleoelevation**.

Sample Dating

Samples collected for 40Ar/39Ar geochronology were processed and dated at the Lehigh University Geochronology Lab. Following crushing, washing and removal of highly magnetic material, several milligrams of fine grained polymineralic groundmass was hand picked for irradiation and subsequent dating. The majority of samples were dated using a total fusion method using a CO2 laser system coupled to an Argus VI noble gas mass spectrometer. Select samples were dated using the step heating method. Data was reduced using ArArCALC.

2013 Mongolia Samples for Vesicular Basalt Paleoaltimetry

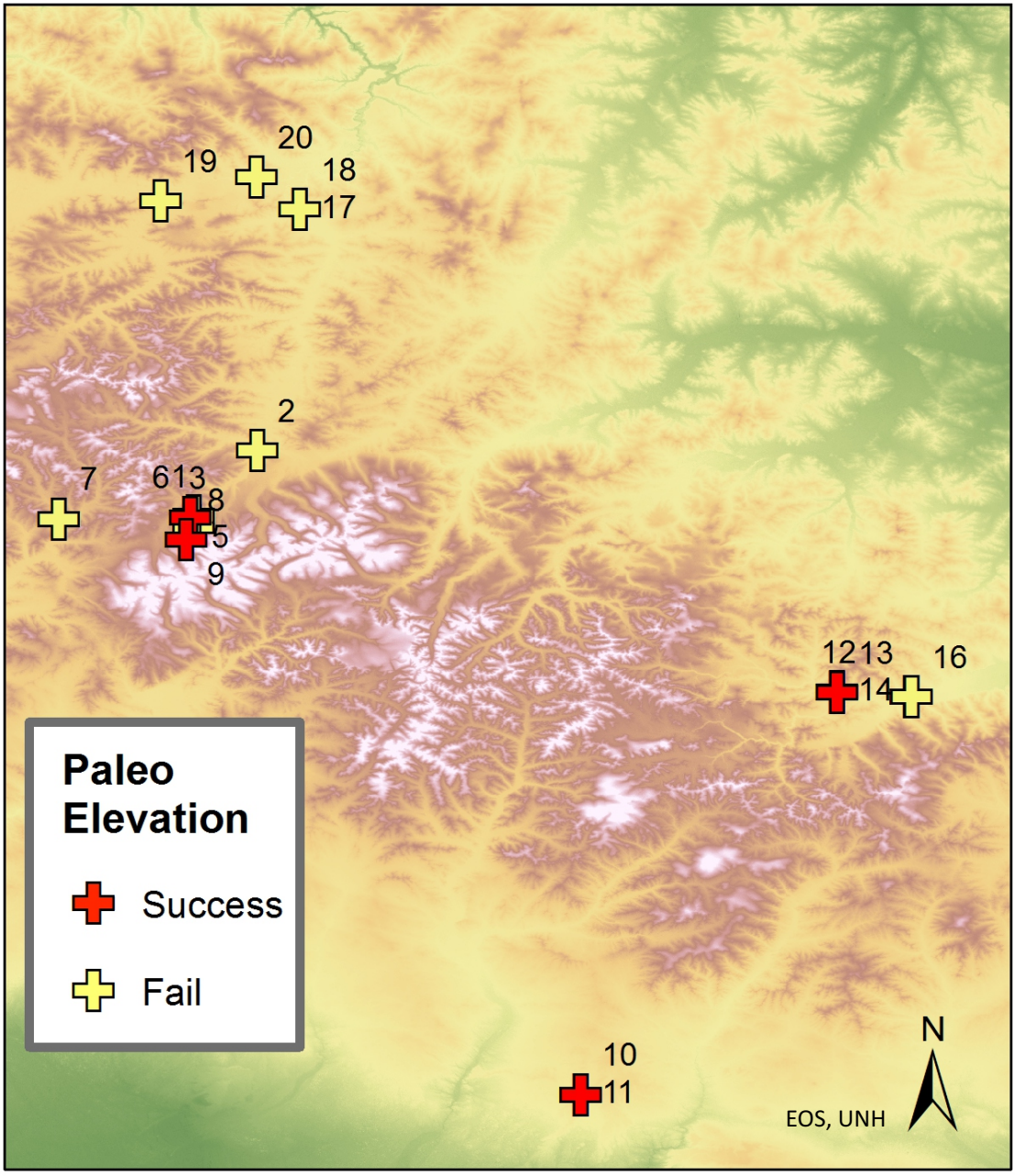

Date	Sample ID	Priority Rating	rating explanation	Location description	AGE	Dating sample	Thickness	Longitude	Latitude	Elevation, m
6/21/2013	DS13-1 (B/T)	2	Some big vesicles in upper zone.	Western slope of Keck camp.			11' 10"	N 47° 16.457'	E 100° 01.812'	2404
6/23/2013	DS13-2 (B/T)	2	thick flow	Western slope of Chulut river		Yes	22' 3"	N 47° 26.886'	E 100° 12.051'	2119
6/23/2013	DS13-3 (B/T)	2	lensy	Upper lensed flow at the top of thick lava flows above keck camp. Lens width = 20 m. Pipe vesicls at the bottom transitional to 2-3 cm diameter bubbly "pipes" at the middle of flow.			7' 3"	N 47° 16.144'	E 100° 01.254'	2443
6/24/2013	DS13-4 (B/T)	4	messed up bottom. Sheared upper vesicles	Messed up caterpillar bottom. Top has sheared vesicles.		yes	12' 4"	N 47° 14.700'	E 100° 01.897'	2524
6/25/2013	DS13-5 (B/T)	2	thin flow	5 and 6 are two thin flows 1.5 km west of keck camp, 20 m west of DS13-3.			31"	N 47° 16.144'	E 100° 01.254'	2443
6/25/2013	DS13-6 (B/T)	1	pretty good	5 and 6 are two thin flows 1.5 km west of keck camp, 20 m west of DS13-3.			4' 2"	N 47° 16.144'	E 100° 01.254'	2443
6/25/2013	DS13-7 (B/T)	3	big upper vesicles	Top section of a stack of flows. Big vesicles? Odd - maybe deflated?			7' 7"	N 47° 15.908'	E 99° 40.081'	2500
6/26/2013	DS13-8 (B/T)	2	big upper vesicles in core	Mouth of tributary on east side of Baytruk river (Campsite #4). Stack of at least 5 lava flows.		yes	7' 7"	N 47° 12.594'	E 100° 00.630'	2240
6/26/2013	DS13-9 (B/T)	1	pretty good	next in stack above DS13-8		yes	7' 5"	N 47° 12.594'	E 100° 00.630'	2240
6/27/2013	DS13-10 (B/T)	3	big upper vesicles	Gobi- stack of several flows total 50 thick. Bottom two flows are massive (10 m thick) with pillows and massive cores. We sampled next two flows.		yes	7' 4"	N 45° 43.006'	E 101° 04.311'	1933
6/27/2013	DS13-11 (B/T)	1	pretty good	next in stack above DS13-10		yes	8' 9"	N 45° 43.006'	E 101° 04.311'	1933
7/2/2013	DS13-12 (B/T)	1	pretty good	Stack of multiple flows on south side of Orkon river valley, above rubble slope. 12 is below 13 and 14.		yes	10' 8"	N 46° 47.994'	E 101° 45.643'	1951
7/2/2013	DS13-13 (B/T)	2	thin flow	middle flow of stack			1' 4"	N 46° 47.994'	E 101° 45.643'	1951
7/2/2013	DS13-14 (B/T)	1	pretty good	top flow of stack		yes	10' 10"	N 46° 47.994'	E 101° 45.643'	1951
7/2/2013	DS13-15 (B/T)	4	thick flow, not well measured [illegible]	Orkon waterfall, near base, below very thick flow.		yes	20' (approx)	N 46° 47.273'	E 101° 57.616'	1793
7/2/2013	DS13-16 (B/T)	[illegible]	[illegible]	[illegible]		[illegible]	[illegible]	[illegible]	[illegible]	[illegible]
7/3/2013	DS13-17 (B/T)	[illegible]	[illegible]	[illegible]		[illegible]	[illegible]	[illegible]	[illegible]	[illegible]
7/3/2013	DS13-18 (B/T)	[illegible]	[illegible]	[illegible]		[illegible]	[illegible]	[illegible]	[illegible]	[illegible]
7/4/2013	DS13-19 (B/T)	[illegible]	not quite top	[illegible]		[illegible]	[illegible]	[illegible]	[illegible]	[illegible]
7/4/2013	DS13-20 (B/T)	[illegible]	pretty good	[illegible]		[illegible]	[illegible]	[illegible]	[illegible]	[illegible]

Sample Analysis

Principles of Vesicular Basalt Paleoaltimetry

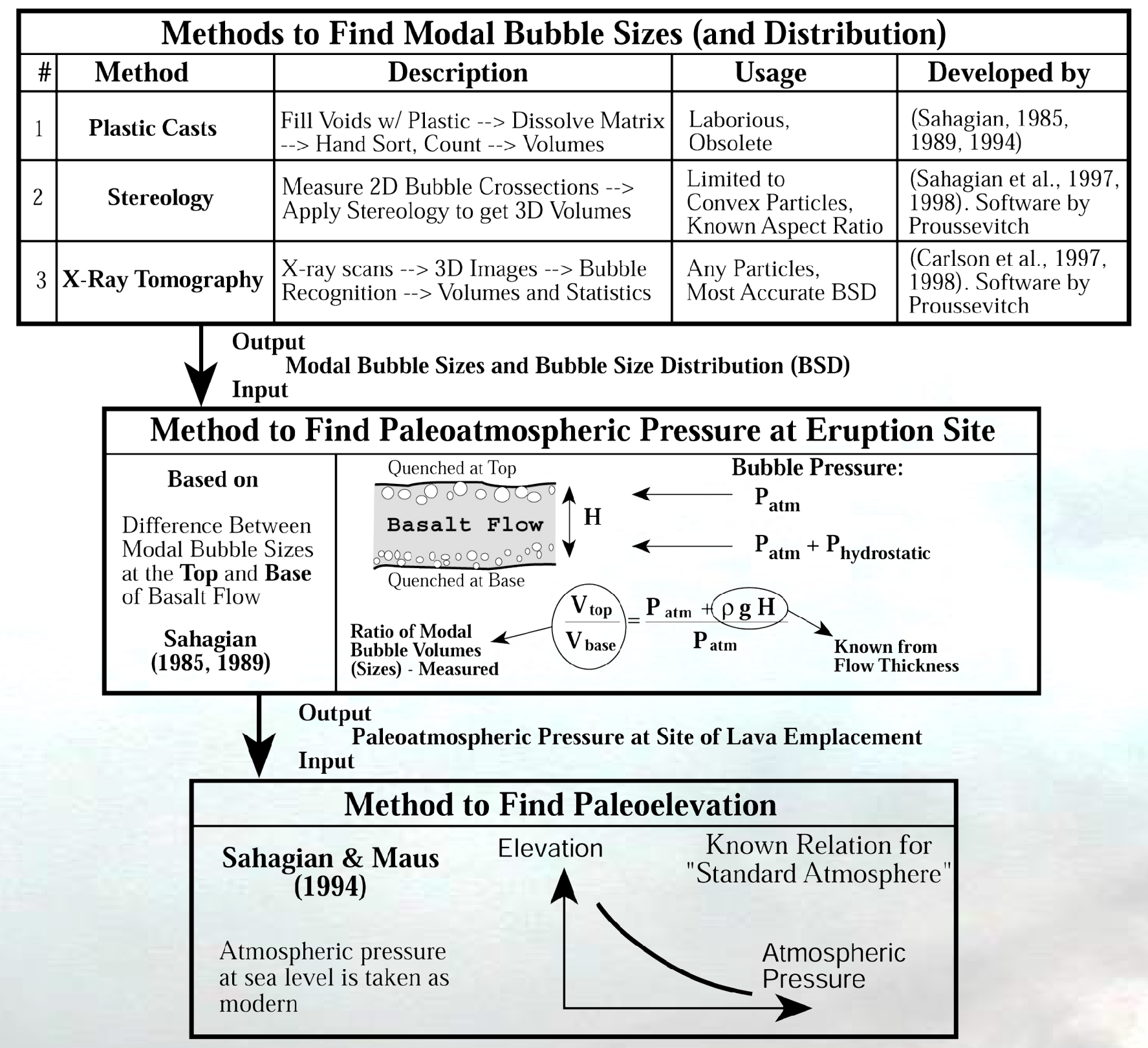

Methods to Find Modal Bubble Sizes (and Distribution)				
#	**Method**	**Description**	**Usage**	**Developed by**
1	**Plastic Casts**	Fill Voids w/ Plastic --> Dissolve Matrix --> Hand Sort, Count --> Volumes	Laborious, Obsolete	(Sahagian, 1985, 1989, 1994)
2	**Stereology**	Measure 2D Bubble Crossections --> Apply Stereology to get 3D Volumes	Limited to Convex Particles, Known Aspect Ratio	(Sahagian et al., 1997, 1998). Software by Proussevitch
3	**X-Ray Tomography**	X-ray scans --> 3D Images --> Bubble Recognition --> Volumes and Statistics	Any Particles, Most Accurate BSD	(Carlson et al., 1997, 1998). Software by Proussevitch

Output
Modal Bubble Sizes and Bubble Size Distribution (BSD)
Input

Method to Find Paleoatmospheric Pressure at Eruption Site

Based on
Difference Between Modal Bubble Sizes at the **Top** and **Base** of Basalt Flow
Sahagian (1985, 1989)

$$\frac{V_{top}}{V_{base}} = \frac{P_{atm} + \rho g H}{P_{atm}}$$

Ratio of Modal Bubble Volumes (Sizes) - Measured
Known from Flow Thickness

Output
Paleoatmospheric Pressure at Site of Lava Emplacement
Input

Method to Find Paleoelevation

Sahagian & Maus (1994)
Atmospheric pressure at sea level is taken as modern

Sample Processing to Determine Paleoelevation

Statistical Analysis for Sample # DS13-6

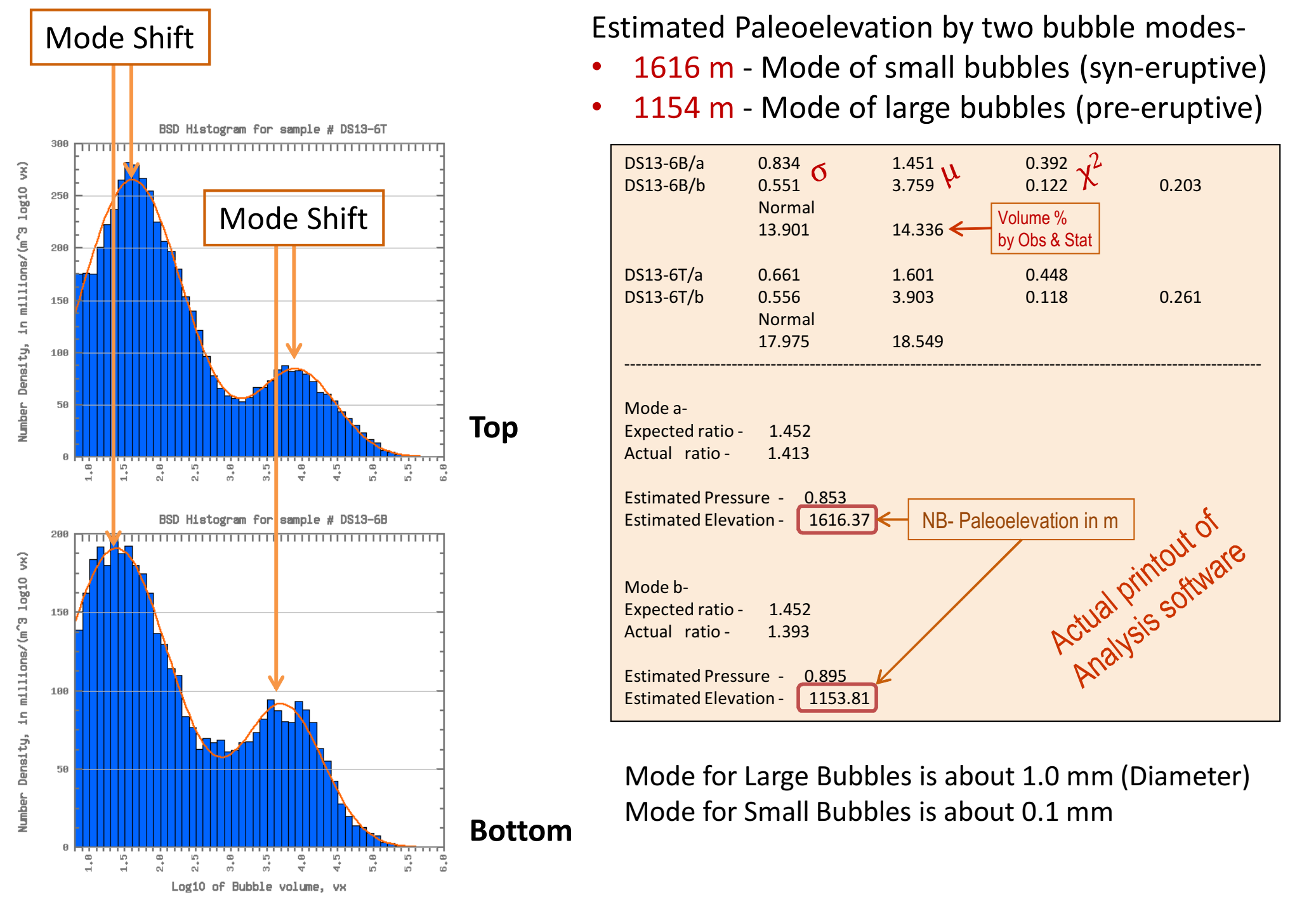

Estimated Paleoelevation by two bubble modes-
- 1616 m - Mode of small bubbles (syn-eruptive)
- 1154 m - Mode of large bubbles (pre-eruptive)

```
DS13-6B/a   0.834     1.451     0.392
DS13-6B/b   0.551     3.759     0.122     0.203
            Normal
            13.901    14.336

DS13-6T/a   0.661     1.601     0.448
DS13-6T/b   0.556     3.903     0.118     0.261
            Normal
            17.975    18.549
--------------------------------------------------------------

Mode a-
Expected ratio -   1.452
Actual   ratio -   1.413

Estimated Pressure  -   0.853
Estimated Elevation -   1616.37

Mode b-
Expected ratio -   1.452
Actual   ratio -   1.393

Estimated Pressure  -   0.895
Estimated Elevation -   1153.81
```

Mode for Large Bubbles is about 1.0 mm (Diameter)
Mode for Small Bubbles is about 0.1 mm

2013 Mongolia Samples for Vesicular Basalt Paleoaltimetry (DS13-6)

Sample # DS13-6
- 1.5 km west of Keck camp
- Thickness: 1.33 m

Sample Processing to Characterize Bubble Population

X-Ray Tomography →

X-Ray Tomography
Non-destructive Image acquisition from rock sample cores is reliable and reproducible. This technology is quite mature and is already widely used for a large number of geological and other applications. For paleoelevation analysis one mandatory condition must be met - each pair of base/top samples should be scanned with the same device settings. Resolution, image fuzziness, beam hardening along the radial direction, etc. can greatly vary, but they always lead to consistent imaging.
This is most reliable and consistent procedure in the analysis.

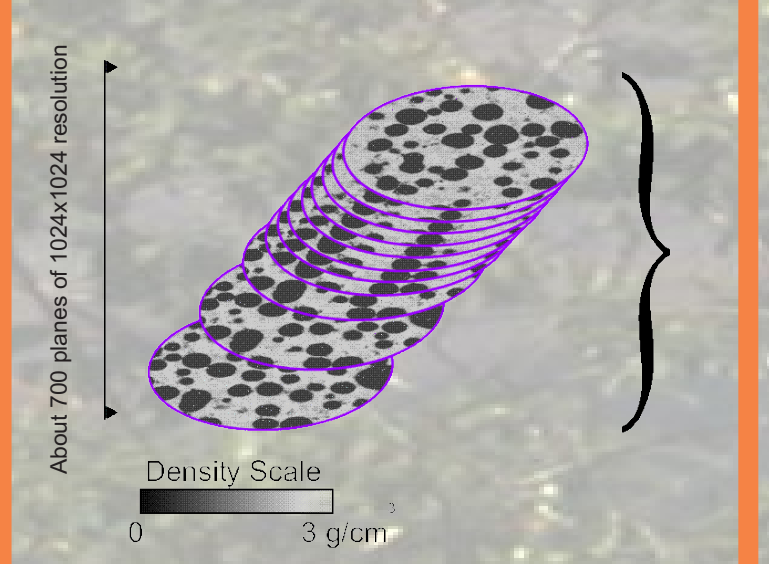

Output from X-Ray Tomography imaging (CT lab at University of Texas) consists of about 700 cross-section planes of 1024x1024 resolution. [illegible]

Dark spots are bubbles in basalt glass and microcrystal matrix shown on light gray background.

[illegible]

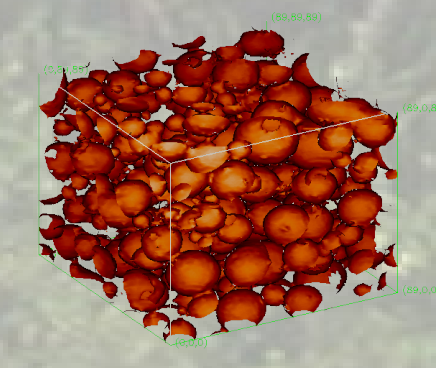
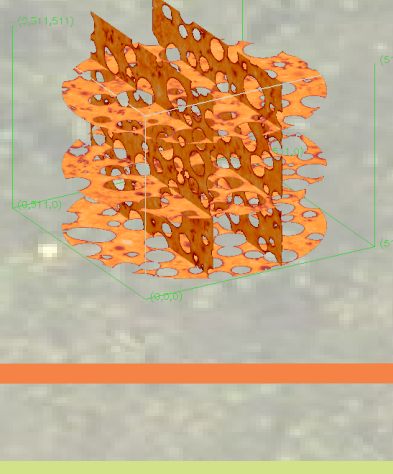

Image Segmentation →

Image segmentation
The most problematic issue in any CXT analysis is how each 3D image element (voxel) is to be physically interpreted. For this quantitative analysis it is a very critical problem. While the center of any bubble and solid glass or crystal texture far from the bubble are clearly distinguishable, there is a range of transitional colors across the bubble/glass interface. The transition zone can be as much as 5 voxels wide, so for small bubbles, uncertainties in defining interface can lead to large errors. The problem gets even more complicated as the segmentation should be done in 3D space. Images that cut the edges of bubbles have extremely wide and blurry margins, rendering application of image segmentation in 2D unreliable. An approach we are using for the segmentation in 3D space is described in the flowchart. For small bubbles, moving the interface by 1 voxel can lead to a doubling or halving of volume. Of course, a consistent procedure for both top/base samples reduces the bubble comparison error.

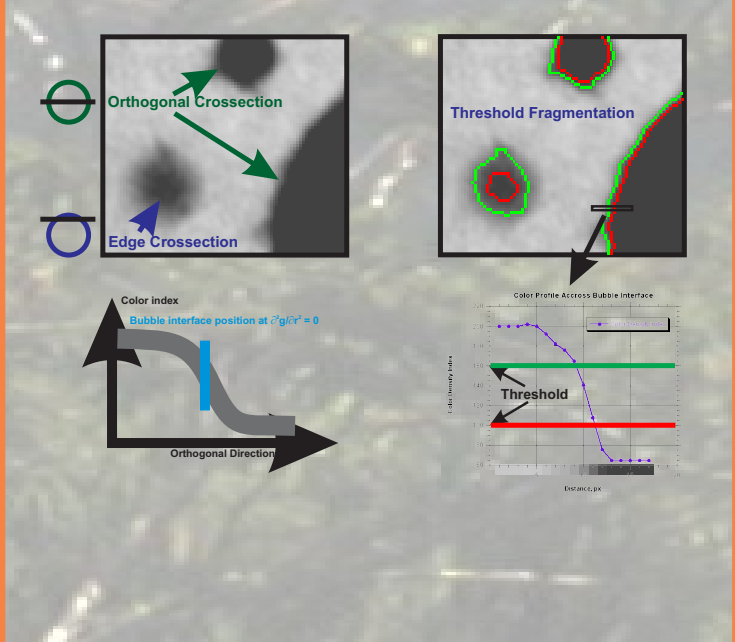

[illegible]

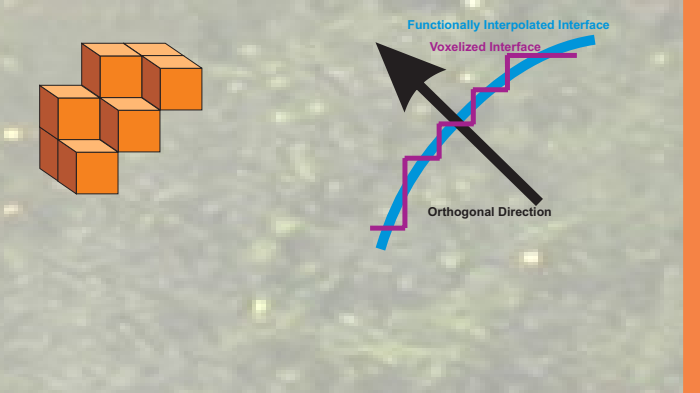

Object Recognition →

Object recognition
The procedure is based on a double pass peeling/reassembly of voxelized structures where each new cluster appearing during reassembly gets a separate identity. The procedure is fast, CPU efficient and conclusive in its results. Only one important control parameter is involved. This is the ratio between the radius of the waist between two bubbles and the radius of the smaller bubble. This ratio must be chosen by the user, depending on the nature [illegible]

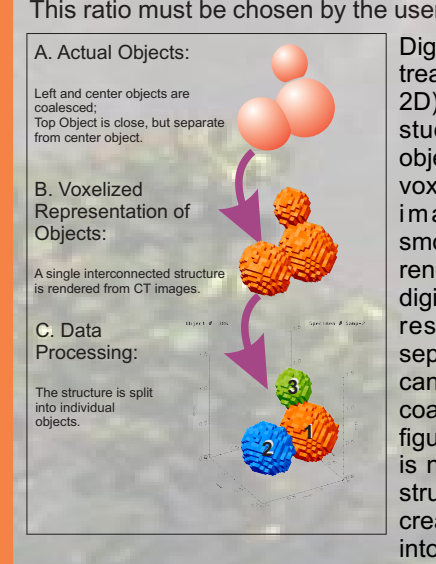

Digitized images are normally treated as a set of pixels (in 2D) or voxels (in 3D). In this study, we considered 3D objects made up of cubic voxels because when digital imagery is generated, smooth-surfaced objects are rendered as such. However, digital imagery often cannot resolve thin films which separate small objects, and it can never separate partially coalesced objects, as in the figure above. Consequently it is necessary to separate the structures of multiple objects created by digital rendering into their component parts.

It would then be possible to then assign identities to each individual object and reassemble the structure. Only in this way can population statistics such as size distribution, interconnectivity, permeability, aspect ratios, and preferred orientation.

a) Actual objects. Two of the objects are partially coalesced and a third is very close but not touching. Both situations lead to [illegible]

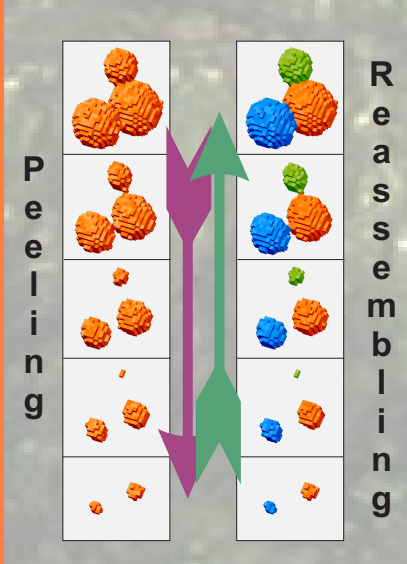

[illegible]

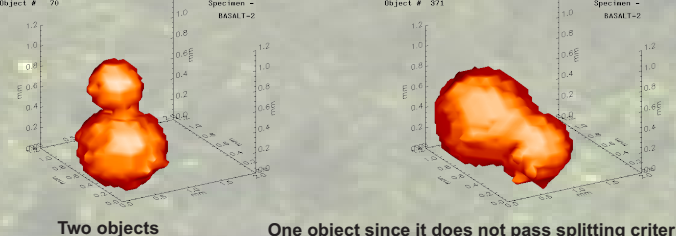

[illegible]

Conclusions for acquisition

Bubble size distributions could be obtained from 2D cross-sections or 3D computed X-Ray tomography (CXT) imagery. These techniques to not directly provide statistical data or numerical characterization of individual bubbles. Consequently, image (2D or 3D) processing for individual bubbles involves segmentation and object recognition -

✎**Segmentation** is the process used to identify each pixel or voxel as void or solid part of the sample. Simple color thresholding proves unsatisfactory, and special methods of color histogram and Kriging analysis often provide better results.

✎**Object recognition** is always required to identify bubbles in the segmented images since they are often interconnected into clusters as continuous void space. Peeling, medial axis analysis, and sphere fitting techniques are currently available to perform this task.

Segmentation and subsequent object recognition of 3D CXT imagery directly provide "true" data for statistical analysis in volumetric (3D) units. Same source data obtained from 2D images represent bubble cross-sections that rarely go through their centers and, thus, do not provide actual bubble sizes. Statistics of 2D cross-sections needs to be converted to actual bubble sizes in 3D. **Stereology** is the field of statistical sciences that is directed to perform the kind of conversion that had been once only applicable to spherical particles. In our previous work we have developed a formulation for stereological analysis of some basic non-spherical shapes, but non-monotonic cross-section frequency functions for these shapes made them virtually impossible to use because cross-section tails (shadows) to smaller classes are larger than their source. So, small observational errors stemming from the inaccurate nature of integer counting for the bins were magnified and made the results impractical.

In this work we have developed a practical approach to bypass the problem with non-monotonic cross-section frequency functions by ignoring classes that are larger than this with maximum probability. Testing of this method on the samples with mono- and bimodal bubble size distributions using 3D CXT data as "true" reference peer showed good match. Mono-modal distribution for moderately deformed bubbles yielded almost perfect match while bimodal distribution for highly deformed bubbles is satisfactory but not yet as good to substitute acquisition in 3D for precision

Results

Paleoelevation and Uplift

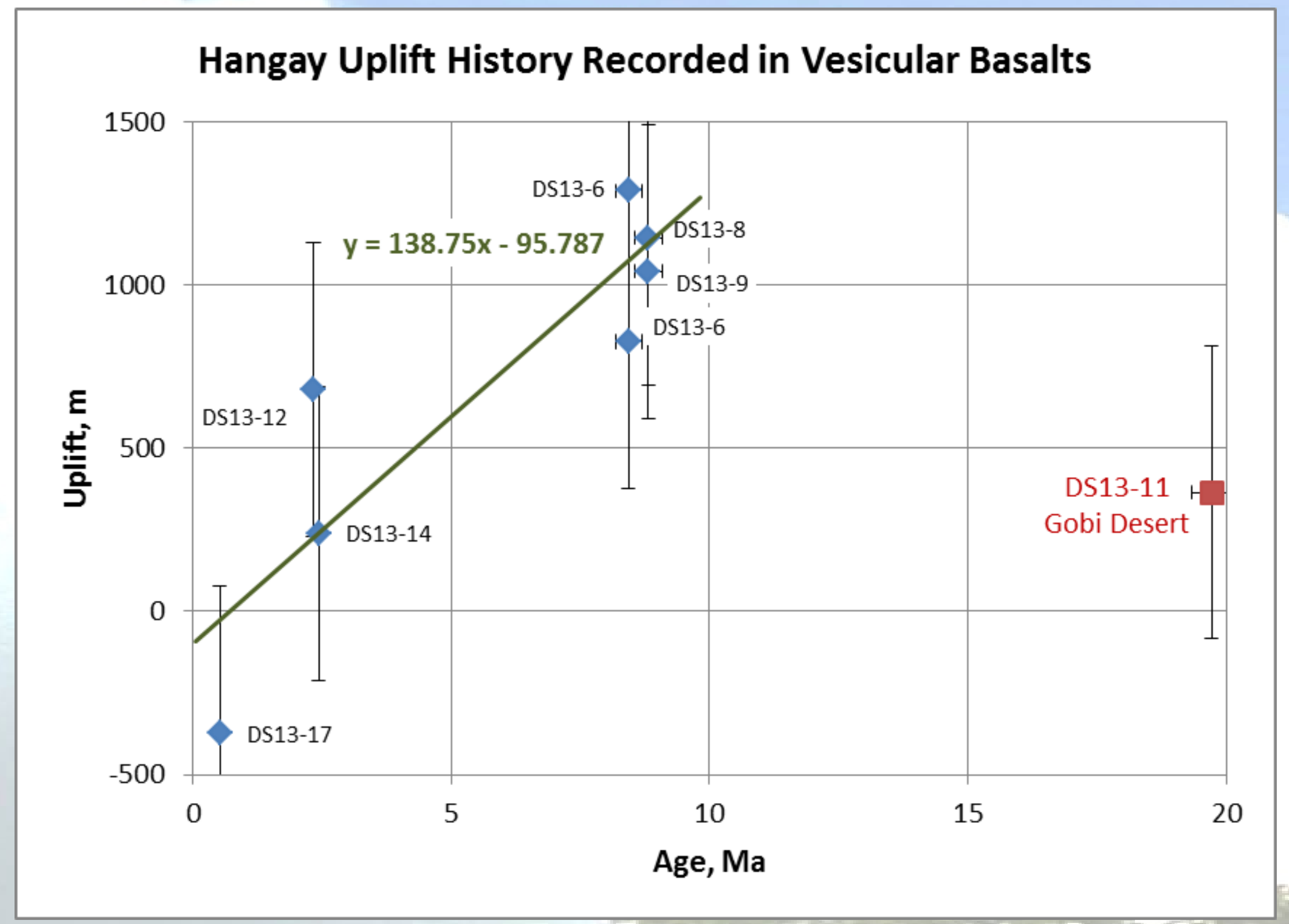

The paleoelevations resulting form analysis of basalt samples collected from throughout the Hangay Plateau indicate about 1 km of uplift in the last 10 million years. While the number of samples is insufficient to resolve acelerations or decelerations of epeirogenic activity, a linear approximation would provide an uplift rate of about 140 m/Ma since the oldest basalts were deposited. The small negative value for DS13-17, a young (0.5 Ma) flow, cannot be distinguished from zero within its error bars, but if the paleoelevation was indeed higher than present, would mean that after a period of uplift, the Hangay recently began to subside, and that the total uplift prior to this was more than measured form the other, uplifted samples. A single, older, sample from the Gobi Desert to the south of Hangay indicates a paleoelevation close to present elevation suggesting that this part of the Gobi did not partake in the uplift experienced by the Hangay.

Sample ID	AGE (Ma)	Present Elevation, m	Calculated Elevation, m	Uplift, m
DS13-6	8.43	2443	1616	827
DS13-6	8.43	2443	1154	1289
DS13-8	8.82	2240	1095	1145
DS13-9	8.82	2240	1198	1042
DS13-12	2.33	1951	1272	679
DS13-14	2.43	1951	1712	239
DS13-17	0.52	1833	2207	-374
DS13-11	19.72	1933	1568	365


Discussion

The overarching goal of this project is to determine the drivers and mechanisms for plateau formation in central Mongolia. The enigmatic nature and position of the Hangay Plateau suggests that heretofore unidentified processes are operating on this part of the Asian lithosphere.

The constraints provided by the vesicular basalts sampled in this part of the project suggest that substantial uplift occurred in the last 10 Ma, rather that being limited to the initial period of India-Asia convergence and mountain-building. As such, more localized mechanisms involving mantle-lithosphere interactions are likely to be playing a role. As results from sister studies involving seismics, geochemistry, geomorphology, isotope systematics, and genetic drift are concatenated, closer constraints on the mechanism of plateau uplift operating in Mongolia should emerge.


Acknowledgments

This material is based upon work supported by NSF under award number EAR-1009680.